



Adsorption of per- and polyfluoroalkyl substances on biochar derived from municipal sewage sludge

Alexis Meservey^a, Indrek Külaots^a, J. Daniel Bryant^b, Chloe Gray^a, Julia Wahl^c, Katherine E. Manz^{a,d}, Kurt D. Pennell^{a,*}

^a School of Engineering, Brown University, Providence, RI, 02912, United States

^b Woodard & Curran, 50 Millstone Road, Building 400, East Windsor, NJ, 08520, United States

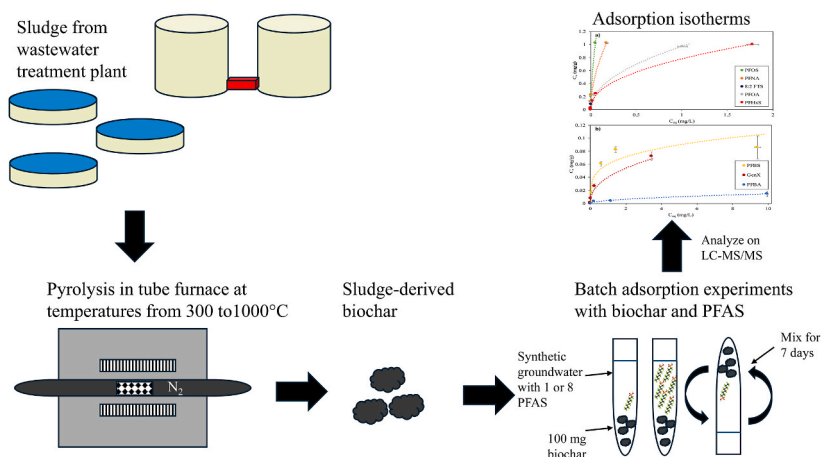
^c Woodard & Curran, 47 Pleasant Street, Northampton, MA, 01060, United States

^d Department of Environmental Health Sciences, School of Public Health, University of Michigan, Ann Arbor, MI, 48109, United States

HIGHLIGHTS

- Biochars were derived from sewage sludge by pyrolysis at 300–1000 °C.
- Adsorption isotherms were measured for eight PFAS on four biochars.
- Biochar surface area and mesoporosity were key factors for PFAS adsorption.
- Adsorption on biochar was dependent on PFAS chain-length and head group.
- Repurposing of sludge into adsorptive biochar offers circular economy benefits.

GRAPHICAL ABSTRACT



ARTICLE INFO

Handling editor: Y Yeomin Yoon

Keywords:

PFAS
Biochar
Freundlich isotherm
Granular activated carbon
Sorption
Sludge

ABSTRACT

Granular activated carbon (GAC) and ion exchange resin (IXR) are widely used as adsorbents to remove PFAS from drinking water sources and effluent waste streams. However, the high cost associated with GAC and IXR generation has motivated the development of less expensive adsorbents for treatment of PFAS-impacted water. Thus, the objective of this research was to create an economically viable and sustainable PFAS adsorbent from sewage sludge. Stepwise pyrolysis at temperatures from 300 °C to 1000 °C yielded biochars whose specific surface area (SSA) and porosity increased from 41 to 148 m²/g, and from 0.062 to 0.193 cm³/g, respectively. On a per organic char basis, the SSA of the biochar was as high as 1183 m²/g, which is comparable to commercially-available activated carbons. The adsorption of perfluorooctane sulfonic acid (PFOS) on sludge biochar increased with increasing pyrolysis temperature, which was positively correlated with increasing porosity and SSA. When 1000 °C processed biochar was tested with a mixture of eight PFAS, preferential adsorption of longer carbon

* Corresponding author. School of Engineering, Brown University, 184 Hope Street, Box D, Providence, RI, 02912, United States.

E-mail address: kurt.pennell@brown.edu (K.D. Pennell).

<https://doi.org/10.1016/j.chemosphere.2024.143331>

Received 28 June 2024; Received in revised form 6 September 2024; Accepted 10 September 2024

Available online 14 September 2024

0045-6535/© 2024 Elsevier Ltd. All rights reserved, including those for text and data mining, AI training, and similar technologies.

chain-length species was observed, indicating the importance of PFAS hydrophobic interactions with the biochar and the availability of a wide range of mesopores. The adsorption of each PFAS was dependent upon both chain length and head group, with longer chain-length species exhibiting greater adsorption than shorter chain-length species, along with greater adsorption of species with sulfonic acid head groups compared to their chain length counterparts with carboxylic acid head groups. These findings demonstrate that biochar derived from municipal solid waste can serve as a cost-effective and sustainable adsorbent for the removal of PFOS and PFAS mixtures from source waters. The circular economy benefits and waste reduction potential associated with the use of sewage sludge-derived biochar supports the development of a viable sludge-derived biochar for the removal of PFAS from water.

1. Introduction

Per- and polyfluoroalkyl substances (PFAS) have been used in a variety of applications, including food packaging, clothing, firefighting foams, and electronics manufacturing (Kissa, 2001; Begley et al., 2005; Glüge et al., 2020). Due to their widespread use and resistance to degradation, there is high potential for human exposure and subsequent risk of adverse health impacts including liver cancer, kidney cancer, and effects on endocrine function, metabolism, and renal health (Abunada et al., 2020; Sinclair et al., 2020; Jha et al., 2021). A primary route for human exposure to PFAS is through the consumption of contaminated food and drinking water (Sinclair et al., 2020; Wisconsin Department of Health Services, 2023). Traditional water treatment methods involving biological or chemical transformation processes have not been effective in completely degrading PFAS to inorganic fluorine (Yu et al., 2009; Appleman et al., 2013; Im et al., 2021; Yadav et al., 2022). As a consequence, current methods to reduce PFAS concentrations to nanogram-per-liter (ng/L) levels in drinking water typically involve the use of adsorbents. Granular activated carbon (GAC) and ion exchange resins (IXRs) are two of the most effective and widely used adsorbents for PFAS removal (United States Environmental Protection Agency, 2022). GAC is generally considered the most cost-effective and common adsorbent used to treat PFAS-impacted water (Yadav et al., 2022). The U.S. EPA recently established Maximum Contaminant Levels (MCLs) of 4 ng/L for perfluorooctanesulfonic acid (PFOS) and perfluorooctanoic acid (PFOA); 10 ng/L for perfluorononanoic acid (PFNA), hexafluoropropylene oxide dimer acid (GenX), perfluorohexanesulfonic acid (PFHxS); and a 1.0 (unitless) hazard index for mixtures of two or more of PFNA, PFHxS, perfluorobutanesulfonic acid (PFBS), and GenX in the final PFAS National Primary Drinking Water Regulation. This will cause an increase in demand for carbon and resin, making alternative adsorbents more attractive in terms of cost and sustainability (United States Environmental Protection Agency, 2023).

GAC is produced from high carbon content materials, including bituminous coal, coconut shell, wood, and lignite coal (Fotouhi and Kresic, 2010), and is an effective adsorbent due to its internal porosity and large specific surface area (United States Environmental Protection Agency, 2018). The process of preparing GAC includes powder palletization, high temperature carbonization, and either chemical or thermal activation (Jjagwe et al., 2021; Soonmin and Kabbashi, 2021), which makes the final product costly and energy-intensive to manufacture (Krahn et al., 2023). GAC can be regenerated through methods such as high temperature incineration and solvent washing, allowing for the reuse of spent GAC rather than replacing it with fresh GAC each time the adsorptive capacity is exhausted (Cantoni et al., 2021). However, high temperatures can cause the pore structure of GAC to deteriorate and operational conditions can negatively impact surface chemistry, further reducing adsorption capacity (Sonmez Baghirzade et al., 2021). Consequently, virgin GAC is often used instead of reactivated GAC in order to achieve better PFAS adsorption performance, while spent GAC is often disposed of via landfilling or incineration.

IXR beads are produced from hydrocarbon polymers that consist of a base polymeric matrix and either positively or negatively charged functional groups (Dixit et al., 2021), allowing for adsorption of both

negatively- and positively-charged contaminants, respectively. When their maximum adsorption capacity has been reached, resins can also be regenerated, most often with solutions containing an organic solvent and brine (Woodard et al., 2017; Boyer et al., 2021). The effectiveness of both GAC and IXRs for the removal of long-chain and short-chain perfluoroalkyl acids (PFAAs), including perfluorosulfonic acids (PFSAs) and perfluoroalkyl carboxylic acids (PFCAs), is strongly dependent on chain length and functional group (Du et al., 2014; Franke et al., 2019; Gagliano et al., 2020; Becanova et al., 2021).

Previous studies have documented the economic, greenhouse gas emission, and energy benefits of using biochar instead of GAC for water purification (Thompson et al., 2016; Krebsbach et al., 2023a). The economic benefit comes from the fact that the use of biochar as an adsorbent eliminates the need for the costly activation process (either chemical or thermal) that all GAC products undergo. Specifically, biochar can be generated with a single-step carbonization process and with lower thermal treatment temperatures, making it a more cost-effective and energy-efficient alternative to either GAC or IXRs (Krebsbach et al., 2023a). Today, biochar is most commonly produced by pyrolyzing biomass or biosolids from sustainable sources, including animal, agricultural, and forestry waste (Alhashimi and Aktas, 2017). However, biochar can also be synthesized from sludge, which is produced in large quantities during the operation of wastewater treatment plants. Sludge has commonly been dried to form biosolids, which were then used for land application as an organic fertilizer on farmland. While this practice is still in use in some areas, it has been stopped or highly restricted in many states because of the presence of PFAS and other pollutants in the biosolids (Hughes, 2023). As a consequence, disposal of sludge and biosolids can be problematic as well as expensive. Due to the potential for methane production, high water content, and contaminants associated with sludge and biosolids, there are risks associated with disposal in landfills, and incineration can be very expensive (Krahn et al., 2023). Keller et al. (2024) investigated the role of pyrolysis in removing contaminants from biosolids and found that overall mass removal of PFAS, pharmaceuticals, and chemicals from personal care products was greater than 99.9%, and removal of microplastics ranged from 91 to 97% dependent upon pyrolysis temperature. Therefore, in addition to lower cost and energy factors, the pyrolysis of sludge to produce biochar allows for the reduction of waste disposal costs at wastewater treatment facilities and circular economy benefits. Pyrolysis is able to remove PFAS in sludge (Sørmo et al., 2023; Keller et al., 2024) and produce a biochar that can subsequently be used to adsorb PFAS, leading to a decreased spending on both waste disposal and adsorbent purchasing for municipal wastewater treatment plants. One of the few studies that investigated the use of sewage sludge biochar for PFAS demonstrated the ability of sewage sludge biochar, pyrolyzed at one temperature, to adsorb PFCAs (Krahn et al., 2023).

Since biochars offer the potential for a more sustainable and economically viable alternative to conventional GAC and IXR, the goal of this study was to systematically investigate the potential of biochars generated from wastewater treatment biosolids (sludge) to adsorb PFOS and PFAS mixtures. Herein, we extensively explore properties of biochars prepared by pyrolysis at temperatures of 300, 600, 900 and 1000 °C for 1 h under a N₂ gas stream. Batch adsorption experiments

were conducted for each biochar with PFOS to obtain baseline adsorption parameters, and the best performing biochar adsorbent generated was subsequently tested with a mixture of eight PFAS to assess competitive adsorption effects over an initial concentration range of 1 $\mu\text{g/L}$ to 5000 $\mu\text{g/L}$. The adsorption data were fit to a Freundlich adsorption model using least squares regression procedures and compared to adsorption data obtained for two reference GACs (DARCO® 12–20 mesh and Filtrasorb® 400).

2. Materials and methods

2.1. Chemicals

PFOS potassium salt (98% purity), PFOA salt (96% purity), PFBS potassium salt (98% purity), PFHxS potassium salt (98% purity), GenX (95% purity), PFNA (97% purity), perfluorobutanoic acid (PFBA) (98% purity), and 8:2 fluorotelomer sulfonic acid (8:2 FTS) (97% purity) were purchased from Sigma-Aldrich (St. Louis, MO). All aqueous solutions were prepared with deionized (DI) water treated with a Milli-Q® Reference Water Purification System (MilliporeSigma, Burlington, MA). Synthetic groundwater (total dissolved solids of 373 mg/L and ionic strength of 8.535 mM) was prepared with magnesium sulfate (Fisher Scientific, Fairlawn, NJ), sodium bicarbonate (Fisher Scientific, Fairlawn, NJ), potassium chloride (Avantor Performance Materials, Center Valley, PA), and calcium chloride (Thermo Fisher Scientific, Waltham, MA). For calibration standards, certified PFAS standards and their and isotope labelled reference standards were purchased from Wellington Laboratories (Overland Park, KS). Isotopically-labelled PFAS were purchased from Wellington Laboratories (Overland Park, KS) for use as internal standard (IS). The IS solution contained mass-labelled PFBA, perfluoropentanoic acid (PFPeA), perfluorohexanoic acid (PFHxA), perfluoroheptanoic acid (PFHpA), PFOA, PFNA, perfluorodecanoic acid (PFDA), perfluoroundecanoic acid (PFUDA), perfluorododecanoic acid (PFDoA), perfluorotetradecanoic acid (PFTeDA), PFBS, PFHxS, and PFOS, each at 2000 ng/L.

2.2. Adsorbents

Biosolids from a municipal wastewater treatment plant were converted to biochar by pyrolysis in a laboratory tube furnace under 300 mL/min N_2 gas flow. Approximately 5 g of biosolids were placed into a porcelain crucible prior to inserting it in the tube furnace. The samples were heated at a rate of 10 °C/min from room to the target temperatures (i.e., 300 °C, 600 °C, 900 °C and 1000 °C) and maintained at this temperature for 1 h. Samples were cooled to room temperature for approximately 1 h under N_2 gas flow (300 mL/min). The resulting material is referred to herein as “biochar”.

Two reference GACs, DARCO® 12–20 mesh GAC and Filtrasorb® 400, were obtained from Sigma-Aldrich (Burlington, MA) and Calgon Carbon Corporation (Pittsburgh, PA), respectively. DARCO® GAC is an acid-washed lignite coal-based carbon with a particle size distribution of 12–20 mesh. Filtrasorb® 400, widely used for drinking water and wastewater treatment, is a reagglomerated bituminous coal-based carbon with a particle size distribution of 12–40 mesh.

2.2.1. Adsorbent characterization

Thermogravimetric analysis (TGA) of the biosolids and biochar samples was carried out using a Mettler Toledo TGA/DSC-1 Star system (Columbus, OH). A similar heating rate to biochar preparation was used (10 °C/min and flow of N_2 gas at 100 mL/min) to determine the organic and mineral contents of the biochars. The biochar SSA and porosity were determined using an Anton-Paar (formerly Quantachrome) Autosorb-1 system (Graz, AT). For these experiments, approximately 20–100 mg of biochar or GAC were placed into a sample bulb and degassed at 300 °C for 24 h. The N_2 adsorption-desorption isotherms were obtained by recording data points at N_2 relative pressures (P/P_0) from 10^{-6} to 1 at a

temperature of 77 K. Specific surface areas were calculated by applying the Brunauer-Emmett-Teller (BET) model and pore size distributions using the non-local density functional theory (NLDFIT) slit pore model (Lastoskie et al., 1993). The pore sizes are presented according to the International Union of Pure and Applied Chemistry (IUPAC) classification, which defines pores less than 2 nm wide as micropores, pores with widths between 2 and 50 nm as mesopores, and pores wider than 50 nm as macropores. Micropore volume and micropore SSA were also determined by applying the Dubinin-Radushkevitch (DR) theory (Lowell et al., 2006). The elemental composition of the biochar was determined using an INNOV-X Systems Alpha 4000 (Woburn, MA) and Olympus Delta Handheld X-ray fluorescence spectroscopy (XRF) DP-600 Premium system (Tokyo, JP) (Table A1). The instrument analyzes elements from Mg to U over a concentration range of 10 mg/L to 10,000 mg/L. An Olympus 316 Standardization Coin for Delta handheld XRF analyzer was used for instrument calibration.

Hydrophobicity of the biochar samples was determined using the ethanol drop test following the procedure described in Edeh and Mašek (2022). The ethanol drop test assesses water repellency using the known surface tensions of ethanol solution at various molarities (Letey et al., 2000; Edeh and Mašek, 2022). Ethanol solutions of 0–6 M were prepared at 0.5 M intervals. Approximately 1.25 g of each biochar was transferred into an aluminum weigh boat (Globe Scientific, Mahwah, NJ) and 5- μL droplets of each ethanol solution were pipetted onto the surface of the biochar. The time for each droplet to be absorbed was recorded using a stopwatch. For each sample, the lowest ethanol concentration that was absorbed in less than 10 s was used to determine hydrophobicity, where hydrophobicity was categorized as hydrophilic (<1 M), hydrophobic (1–2 M), strongly hydrophobic (2–3.5 M), and extremely hydrophobic (>3.5 M) (Kinney et al., 2012; Edeh and Mašek, 2022).

2.3. Batch adsorption experiments

For initial batch reactor adsorption tests, 10 mL of synthetic groundwater containing PFOS at 7 initial concentrations over a concentration range of 0.1 $\mu\text{g/L}$ to 10,000 $\mu\text{g/L}$ was mixed with ca. 100 mg of biochar in 15 mL polypropylene centrifuge tubes (Thermo Fisher Scientific, Waltham, MA). After the initial PFOS adsorption tests, batch reactor adsorption tests with 10 mL of synthetic groundwater containing a mixture of 8 PFAS (PFOS, PFOA, PFBS, PFHxS, GenX, PFNA, PFBA, and 8:2 FTS at equal mass concentrations) or single solute PFBS, PFHxS, and GenX, over a concentration range of 1 $\mu\text{g/L}$ to 2500 $\mu\text{g/L}$, were mixed with ca. 100 mg of the biochar that exhibited the greatest adsorption of PFOS in 15 mL polypropylene centrifuge tubes. Triplicate batch reactors were prepared for each PFAS concentration along with triplicate controls without biochar. The reactors were mixed on a Thermo Scientific™ Tube Revolver Rotator (Thermo Fisher Scientific, Waltham, MA) at 30 rpm for 14 days. After mixing, the reactors were centrifuged in an Eppendorf 5804 R centrifuge (Eppendorf North America, Enfield, CT) at 3000 rpm for 30 min. Two mL of supernatant were transferred to Fisherbrand™ microcentrifuge tubes (Thermo Fisher Scientific, Waltham, MA) and subject to centrifugation at 15,000 rpm for 15 min in an Eppendorf 5424 centrifuge (Eppendorf North America, Framingham, MA). After centrifugation, the supernatant was transferred to a Waters™ 2 mL clear glass vial, diluted to appropriate concentration ranges for targeted PFAS analysis, and spiked with IS so that it comprised 10% of each of the prepared samples. The resulting PFAS data were fit to the Freundlich model using a non-linear least-squares regression procedure in Python. For comparison purposes, batch adsorption experiments were conducted in the same manner for PFOS and the two reference carbons (DARCO® 12–20 mesh GAC and Filtrasorb® 400).

2.3.1. PFAS analysis

Targeted PFAS analysis was carried out using a Waters Acquity UPLC H-class system connected to a Waters Xevo TQ-S Micro triple-quadrupole mass spectrometer (Milford, MA). An Acquity UPLC BEH

C18 column (2.1 mm × 50 mm × 1.7 μm) (Waters, Milford, MA) at 50 °C was used for the separation of analytes. Mobile phase A consisted of 2 mM ammonium acetate (Sigma-Aldrich, Burlington, MA) in 5% methanol (Fisher Scientific, Fairlawn, NJ) and mobile phase B consisted of 2 mM ammonium acetate in 100% methanol. For the separation of analytes, 10% B was held for 1.2 min, followed by a linear gradient of 10% B to 85% B from 1.2 min to 17 min, then a 0.5-min linear ramp to 100% B, followed by an immediate linear decline to initial conditions for equilibrium over 0.5 min. A modified 10-min gradient program was used during analyses of less than three analytes. Quantification was performed using an external seven-point calibration curve prepared by serial dilution of the calibration standards. The calibration curves were produced within Waters Targetlynx Application Manager for MassLynx software through plotting the peak area ratio, defined by analyte/internal standard, for each calibration point. The Limits of Detection (LOD) were determined following the US EPA's procedure at 40 CFR part 136, Appendix B: seven injections of calibration standards and multiplying the standard deviation of these injections by 3.143 ($t_{0.99}$ at 6° freedom) divided by the calibration curve slope. The measured LODs for the eight PFAS in the mixture were: 10.03 ng/L GenX, 20.38 ng/L PFBS, 91.75 ng/L PFOS, 35.70 ng/L PFOA, 23.36 ng/L PFHxS, 17.83 ng/L PFNA, 21.63 ng/L PFBA, and 73.33 ng/L 8:2 FTS.

3. Results and discussion

3.1. Effect of pyrolysis temperature on biochar characteristics

Biochar properties, including organic char content, porosity, and surface area, are presented as a function of pyrolysis temperature in Table 1.

As the pyrolysis temperature was increased, the organic char content (primarily carbon) of the biochar decreased from 32.0% at 300 °C to 16.3% when heated at 1000 °C. This trend was expected for biochar pyrolysis since more organic matter will be volatilized at higher temperatures. The biochar BET specific surface area (SSA) increased from 41 m²/g to 148 m²/g as the pyrolysis temperature was increased from 300 °C to 1000 °C. However, when the SSA was expressed on organic char bases, the SSA increased from 125 m²/g to 1183 m²/g. Thus, the biochar SSA value per organic char at 1000 °C is comparable to the SSA for commercial activated carbons. The DR and DFT SSA values are in excellent agreement with the BET SSA values, suggesting that the multi-layer N₂ adsorption on biochars (BET model assumption) is valid. The observed increase in SSA with pyrolysis temperature was attributed to the increase in micropores from 0.012 cm³/g-total to 0.054 cm³/g-total and smaller size mesopores (2.5–4.5 nm) (see Table 2, PSD in Fig. A1). An increase in sample porosity and SSA during the carbonization step (pyrolysis) is not unusual. For example, a similar increase in the SSA of biochar derived from waste timber with increasing pyrolysis temperature was reported by Sørmo et al. (2021) however, only pyrolysis temperatures of 800 °C and 900 °C were considered.

Table 1

Biochar and reference activated carbon organic char contents, BET, DR and DFT surface areas, micro, meso and macro, and total porosities obtained from N₂ adsorption isotherms measured at 77 K.

Adsorbent	Organic char content (%)	BET area (m ² /g -total)	BET area (m ² /g -char)	Total Pore Volume (cm ³ /g)	DR Micropore Volume (cm ³ /g)	Meso and Macropore Volume (cm ³ /g)	DR area (m ² /g total)	DFT area (m ² /g-total)
300 °C Biochar	32.0	41	125	0.062	0.012	0.050	33	28
600 °C Biochar	31.4	113	358	0.138	0.043	0.095	117	112
900 °C Biochar	22.7	103	447	0.095	0.038	0.057	107	103
1000 °C Biochar	16.3	148	1183	0.193	0.054	0.139	154	141
DARCO® GAC	78.0	550	705	0.670	0.200	0.470	550	528
Filtrosorb® 400 GAC	86.0	1207	1403	0.721	0.630	0.091	1207	1003

Table 2

Reported PFOS adsorption capacities based on the Langmuir model for ion-exchange resins, activated carbons, and biochars.

Adsorbent	Initial PFOS Concentration (mg/L)	Adsorption Capacity (mg/g)	References	
Ion Exchange Resins	Purolite A520E	1000	210.4	Zaggia et al. (2016)
	Purolite A532E	1000	260.5	Zaggia et al. (2016)
	Purolite A600E	1000	186.2	Zaggia et al. (2016)
	AS-F 520		1988.3	Schuricht et al. (2017)
AS-L K6362		314.9	Schuricht et al. (2017)	
IRA910		1350.2	Maimaiti et al. (2018)	
IRA67		2390.0	Gao et al. (2017)	
Granular Activated Carbons	GAC	10	72.2	Zhang et al. (2016)
	GAC	20–250	274.0	Yu et al. (2009)
	Calgon F400	15–150	236.4	Ochoa-Herrera and Sierra-Alvarez (2008)
Biochars	Saw dust-derived biochar	0.5–325	178.1	Hassan et al. (2020)
	Maize straw biochar (M400)	1–500	164.0	Chen et al. (2011)
	Commercial Douglas fir biochar	1–60	7.0–14.6	Rodrigo et al. (2022)
	Corn straw-derived biochar	0.5–10	135.5–169.3	Guo et al. (2017)
	Commercial Douglas fir-derived biochar	0.01–4	42.3	Krebsbach et al. (2023b)
	0.01–4	4.97	Krebsbach et al. (2023b)	

3.2. Effect of biochar pyrolysis temperature on PFOS adsorption

Single analyte (PFOS) batch adsorption experiments were conducted with biochar treated at 300, 600, 900, and 1000 °C. For each of the biochars, PFOS adsorption data exhibited non-linear behavior, and were fit to the Freundlich model $C_s = K_F C_{eq}^n$, where C_s is the solid-phase concentration, C_{eq} is the aqueous phase concentration, K_F is the Freundlich distribution coefficient, and n is the adsorption constant (Liu et al., 2022). The Freundlich adsorption parameters for each of the PFOS batch adsorption experiments are shown in Table A2. Biochar processed at 300 and 600 °C exhibited the lowest adsorption of PFOS, with PFOS adsorption increasing greatly as pyrolysis temperature was increased above 600 °C (Fig. 1). The observed increase in PFOS adsorption corresponded to the greater hydrophobicity of the biochar at pyrolysis temperatures of 900 °C and 1000 °C (Table A3).

Results shown in Table 2 suggest similar SSA and porosity for 600 °C

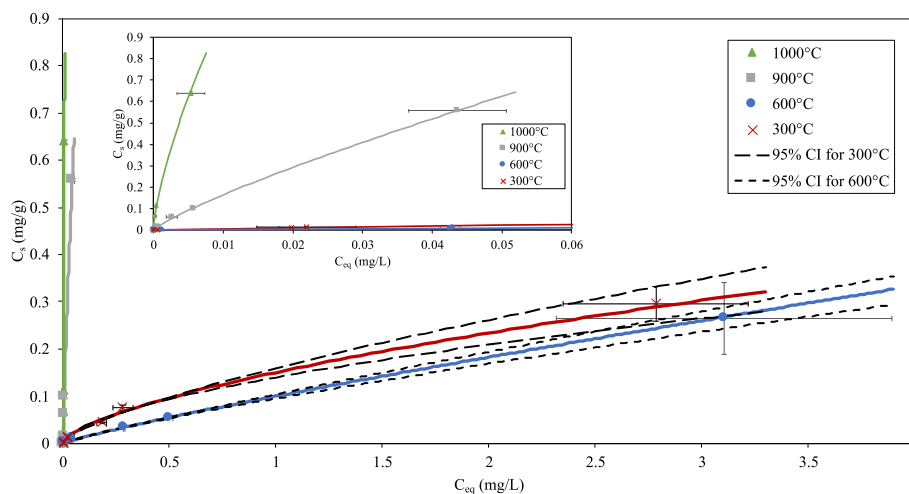


Fig. 1. a) Freundlich adsorption isotherms for PFOS on 1000 °C biochar, 900 °C biochar, 600 °C biochar, 300 °C biochar, and untreated biochar. Insert shows adsorption isotherms up to $C_{eq} = 0.06$ mg/L.

and 900 °C prepared biochar samples, but the main difference between PFOS adsorption (Fig. 1) can be explained by the pore size distribution (PSD) differences between the 600 °C and 900 °C biochar samples. Here, the greater PFOS adsorption was attributed to the greater fraction of mesopores (i.e., ≥ 4 nm) present in the 900 °C biochar. Previous studies have reported the importance of porosity and surface area in the adsorption of PFAS by biochars (Kundu et al., 2021; Sørmo et al., 2021; Krahn et al., 2023). For example, the 1000 °C biochar, which had the largest surface area and volume of mesopores, exhibited the greatest adsorption of PFOS. Additionally, porosity and SSA play a more important role in the adsorption of PFOS than organic char content, as demonstrated by the 1000 °C biochar having the lowest organic char content. A correlation was developed between the adsorption of PFOS and the SSA and meso- and macropore volume of the biochars (see Fig. A2). The correlation obtained is the following: $C_s = -0.0282 * SSA + 45.102 * MMPV - 1.089$, where SSA is the specific surface area and MMPV is the meso- and macropore volume, suggesting that SSA and meso- and macropore volume can be used as predictors for PFOS adsorption ($R^2 = 0.999$).

The adsorption of PFOS onto the 1000 °C biochar was also compared to adsorption onto two reference activated carbons, DARCO® GAC and Filtrasorb® 400 (Figs. A3 and A4). On a total mass basis, the adsorption of PFOS on the biochar was less than that of the two reference carbons, with Filtrasorb® 400 exhibiting the greatest adsorption. For example, at an equilibrium aqueous phase concentration of 10 $\mu\text{g/L}$, the amount of PFOS adsorbed to the 1000 °C biochar was 1010.8 $\mu\text{g/g}$, compared to 4526.0 $\mu\text{g/g}$ and 7585.8 $\mu\text{g/g}$ for DARCO® GAC and Filtrasorb® 400, respectively. This difference was attributed to the much larger specific surface area (1207 m^2/g for Filtrasorb® 400 vs. 550 m^2/g for DARCO® GAC vs. 148 m^2/g for 1000 °C biochar) and the greater total pore volume (0.721 cm^3/g for Filtrasorb® 400 vs. 0.670 cm^3/g for DARCO® GAC vs. 0.193 cm^3/g for 1000 °C biochar) of Filtrasorb® 400 (Table 2). However, it should be noted that when PFOS adsorption is expressed on a per organic char basis the adsorption values obtained for 1000 °C biochar and DARCO® GAC are similar (5803 $\mu\text{g/g}$ char vs. 6201 $\mu\text{g/g}$ char).

3.3. Comparison of PFOS adsorption by municipal sludge biochar and other adsorbents

In a comparison of reported PFOS adsorption capacities for IXRs, GAC, and biochars (Table 2) (Rodrigo et al., 2022; Yadav et al., 2022), the highest reported adsorption capacities were associated with IXRs. However, some biochar adsorption capacities compared well to values

reported for GAC and IXR.

Freundlich adsorption parameters reported for biochars prepared from different source materials exhibit a range of PFOS adsorption capacities (Table 3).

The 1000 °C sludge biochar exhibited greater or similar adsorption of PFOS when compared to many other types of biochars but had lower adsorption than the corn-straw derived biochars (Fig. A5). Similar to our observations of higher PFOS adsorption as pyrolysis temperature increased, Deng et al. (2015) and Guo et al. (2017) reported increases in PFOS adsorption with increasing pyrolysis temperature for bamboo- and corn straw-derived biochars, respectively. The adsorption capacity of the corn straw-derived biochar, determined from fitting data to the Langmuir adsorption isotherm, increased from 135.53 mg/g at 250 °C to 169.30 mg/g at 700 °C (Guo et al., 2017). Additionally, both studies reported increased pore volume, specifically in the mesopore range, with increasing pyrolysis temperature. The increased surface area and total pore volume of the corn straw-derived biochar likely played a role in the greater adsorption capacity of PFOS at higher pyrolysis temperatures. At an aqueous phase concentration of 10 $\mu\text{g/L}$, PFOS adsorption onto the different biochars ranged from 280.3 to 2572.9 $\mu\text{g/g}$, with our 1000 °C sludge biochar adsorbing 649.0 $\mu\text{g/g}$. Unfortunately, many of these studies did not report detailed biochar characterization data, such as micro- and mesoporosity, and thus, we were not able to expand the PFOS adsorption correlation presented above and more thoroughly investigate relationships between specific biochar properties and PFOS adsorption.

Table 3

Comparison of reported Freundlich adsorption parameters for PFOS onto biochar.

Biochar	$K_F \left[\frac{\text{mg L}^{-n}}{\text{g mg}} \right]$	n	References
1000 °C sludge biochar	25.39	0.70	Present study
400 °C willow-derived biochar	5.23	0.49	Chen et al. (2011)
400 °C maize-derived biochar	7.27	0.46	Chen et al. (2011)
600 °C unmodified sawdust biochar	4.24	0.59	Hassan et al. (2020)
600 °C red mud modified sawdust biochar	5.98	0.55	Hassan et al. (2020)
900 °C bamboo biochar	3.20	0.29	Deng et al. (2015)
250 °C corn straw-derived biochar	58.61	0.83	Guo et al. (2017)
400 °C corn straw-derived biochar	68.99	0.82	Guo et al. (2017)
550 °C corn straw-derived biochar	83.14	0.81	Guo et al. (2017)
700 °C corn straw-derived biochar	97.82	0.79	Guo et al. (2017)

3.4. Adsorption of a PFAS mixture by municipal sludge biochar

Batch adsorption experiments were performed with the 1000 °C biochar and equal mass concentration mixtures of eight PFAS (PFOS, PFOA, PFBS, PFHxS, GenX, PFNA, PFBA, and 8:2 FTS), as well as single solute PFBS, PFHxS, and GenX, to investigate potential competitive adsorptive effects, which have been observed previously for carbons and resins (Appleman et al., 2014; Xiao et al., 2017; Cantoni et al., 2021; Murray et al., 2021; Riegel et al., 2023). The adsorption data for each PFAS were fit to the Freundlich adsorption model using a non-linear least-squares regression approach. The 1000 °C biochar was most effective at removing long-chain PFAS compounds, with the greatest adsorption observed for PFOS, followed by PFNA, 8:2 FTS, PFOA, and PFHxS. At a C_{eq} of 10 $\mu\text{g/L}$, C_s values of 384.9, 224.7, 177.1, 106.4, and 102.8 $\mu\text{g/g}$ were obtained for PFOS, PFNA, 8:2 FTS, PFOA, and PFHxS, respectively. The removal of shorter-chain compounds (GenX, PFBS, and PFBA) was much lower, with PFBA exhibiting the lowest adsorption (Fig. 2, Table A4).

The C_s values obtained for GenX, PFBS, and PFBA at a C_{eq} of 10 $\mu\text{g/L}$ were 5.5, 19.0, and 0.4 $\mu\text{g/g}$, respectively. The adsorption of the PFAS

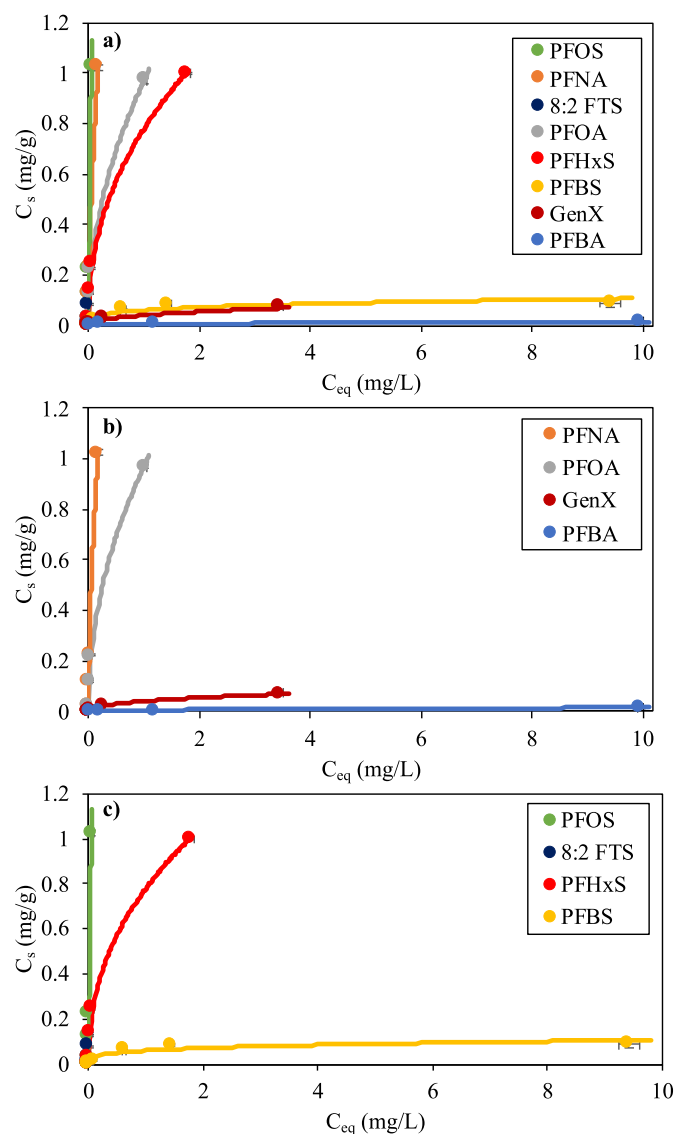


Fig. 2. Freundlich adsorption isotherms obtained for a) 1000 °C biochar and PFOS, PFOA, PFBS PFHxS, GenX, PFNA, PFBA, and 8:2 FTS; b) 1000 °C biochar and the carboxylates (PFOA, GenX, PFNA, and PFBA); and c) 1000 °C biochar and the sulfonates (PFOS, PFBS PFHxS, and 8:2 FTS).

followed a general trend with respect to the chain length of the molecules, with adsorption decreasing as chain length decreased. These results are consistent with previously reported adsorption data for PFAS mixtures on GACs, IXRs, and biochars (Ochoa-Herrera and Sierra-Alvarez, 2008; Hansen et al., 2010; Medina et al., 2022; Krahn et al., 2023; Riegel et al., 2023). For a biochar derived from sewage sludge, Krahn et al. (2023) reported greater adsorption of longer-chain length PFCAs from a mixture of six (PFPeA, PFHxA, PFHpA, PFOA, PFNA, and PFDA), which is consistent with our outcomes.

The greater adsorption of longer-chain length PFAS in the mixture is attributed to the increased hydrophobicity of individual PFAS as the C–F chain length increases (Ochoa-Herrera and Sierra-Alvarez, 2008; Hansen et al., 2010; Medina et al., 2022; Riegel et al., 2023). Therefore, PFAS with longer C–F chain lengths are more hydrophobic than compounds with shorter C–F chain lengths, leading to a lower affinity for the aqueous solution and greater hydrophobic interactions with the biochar. The hydrophobicity of the 1000 °C biochar was evaluated using an ethanol drop test (Table A3), which indicated that the biochar was extremely hydrophobic. The hydrophobicity test results provide further evidence that hydrophobic interactions were the dominant mechanism contributing to adsorption of PFAS onto the biochar. This indicates the importance of polarity in the adsorption of PFAS onto biochar (Sormo et al., 2021, 2023) or any carbon-based adsorbent material. The functional head group of the PFAS (carboxylate versus sulfonate) appears to play a secondary role in the observed adsorption performance. Consistent with the hydrophobicity effect discussed above, PFAS with a sulfonic acid head group exhibited slightly greater adsorption than their equivalent chain length counterparts with carboxylic acid head groups (e.g., PFOS vs. PFOA and PFBS vs. PFBA) (Fig. 3).

This behavior has been observed in prior studies on adsorption of PFAS mixtures by both IXRs and GACs (Ochoa-Herrera and Sierra-Alvarez, 2008; Appleman et al., 2014; Du et al., 2014; Zaggia

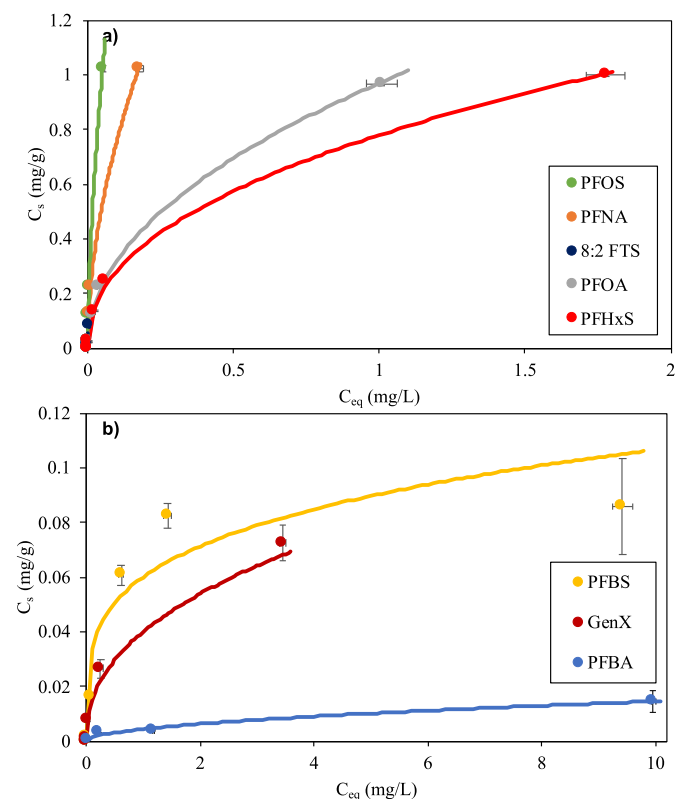


Fig. 3. Freundlich adsorption isotherms obtained for a) 1000 °C biochar and the long chain-length PFAS (PFOS, PFOA, PFHxS, PFNA, and 8:2 FTS); b) 1000 °C biochar and the short chain-length PFAS (PFBS, PFBA, and GenX).

et al., 2016; McCleaf et al., 2017; Riegel et al., 2023), as well as other biochars (Askeland et al., 2020; Sørmo et al., 2021).

For the 1000 °C biochar, competitive adsorption effects were observed for each of the sulfonate compounds (PFOS, PFBS, PFHxS, and GenX) when in solution with other PFAS (PFOS, PFOA, PFBS, PFHxS, GenX, PFNA, PFBA, and 8:2 FTS). This effect can be seen by comparing the adsorption of each of the sulfonate compounds onto the biochar when in a single solute solution versus in a solution with a mixture of eight PFAS (Fig. 4).

Competition between the PFAS compounds for adsorption sites on the biochar led to decreased adsorption of the compounds, with the largest effect being on the compound with the shortest chain length (PFBS). This is likely due to the greater affinity of the longer-chain compounds to the biochar, causing their preferential adsorption over the shorter-chain compounds.

Krahn et al. (2023) also demonstrated the potential use of biochar produced from sludge as an adsorbent for the treatment of PFCAs (PFPeA, PFHxA, PFHpA, PFOA, PFNA, and PFDA), singly and as a mixture, in water and soil. Their two biochars, produced from dewatered sewage sludge and the digestate from anaerobically digested sludge and food waste, exhibited adsorption for six individual PFCAs at ranges from 58.9 to 11,481.5 µg/g and 25.7–1659.6 µg/g, respectively, at an aqueous phase concentration of 10 µg/L. Their results exhibited similar trends in increasing adsorption with increasing PFAS chain length, indicating that hydrophobic interactions were an important sorption mechanism for these biochars. The pyrolysis of two types of sludge at 700 °C produced biochars with SSAs of 262 and 171 m²/g, and meso- and macropore volumes of 0.153 and 0.133 cm³/g, respectively, compared to our SSA of 148 m²/g and MMPV of 0.139 cm³/g for the 1000 °C biochar. Additionally, both sludge biochars had similar elemental compositions to our biochar.

4. Conclusions

This study provides experimental data to support the feasibility of using sludge-derived biochars for the treatment of PFAS-impacted water. Biochar produced from wastewater treatment plant sludge offers sustainability and cost benefits, including a reduction in both biochar production and waste disposal costs, as well as decreased greenhouse gas emissions if compared to the conventional GAC and IXR adsorbents used for PFAS removal. The SSA and porosity of the sludge were shown to be positively correlated with increasing pyrolysis temperature. These properties played a key role in the adsorption of PFAS, as evidenced by the greatest adsorption of PFOS on the 1000 °C biochar, which had the largest SSA and mesoporosity. The 1000 °C sludge biochar was able to effectively remove long-chain PFAS compounds (PFOS, PFOA, PFNA, PFHxS, and 8:2 FTS), and showed preferential adsorption for PFASs over PFCAs. In addition to SSA and porosity, the longer chain length PFAS provide needed hydrophobic surface interactions which enhance overall PFAS adsorption. The use of sludge-derived biochar offers a beneficial circular economy approach for wastewater treatment plants to repurpose their waste stream to treat long-chain PFAS-impacted wastewater. Additional studies are warranted to identify specific biochar properties or amendments that can be used to further enhance PFAS adsorption.

CRedit authorship contribution statement

Alexis Meservey: Writing – original draft, Visualization, Software, Project administration, Methodology, Investigation, Formal analysis. **Indrek Külaots:** Writing – original draft, Visualization, Investigation, Formal analysis. **J. Daniel Bryant:** Writing – review & editing, Resources, Project administration, Methodology, Funding acquisition,

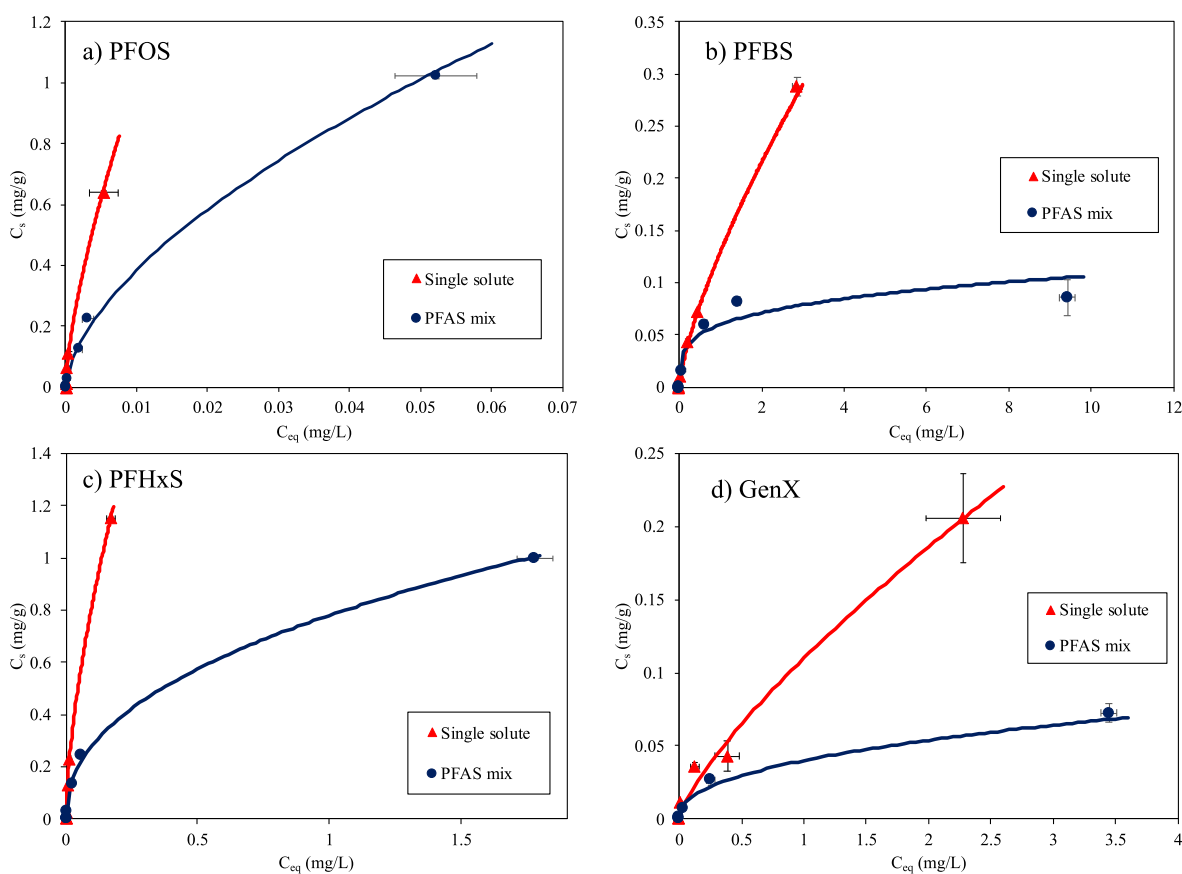


Fig. 4. Comparisons of Freundlich adsorption isotherms obtained for 1000 °C biochar with a) PFOS; b) PFBS; c) PFHxS; d) GenX individually and as a mixture of eight PFASs.

Conceptualization. **Chloe Gray:** Investigation. **Julia Wahl:** Writing – review & editing, Project administration, Conceptualization. **Katherine E. Manz:** Writing – review & editing, Supervision. **Kurt D. Pennell:** Writing – review & editing, Supervision, Resources, Project administration, Methodology, Funding acquisition.

Declaration of competing interest

The authors declare the following financial interests/personal relationships which may be considered as potential competing interests:

Kurt Pennell reports financial support was provided by Strategic Environmental Research and Development Program. Kurt Pennell reports financial support was provided by Woodard & Curran. Kurt Pennell reports a relationship with United States Environmental Protection Agency that includes: funding grants. If there are other authors, they declare that they have no known competing financial interests or personal relationships that could have appeared to influence the work reported in this paper.

Data availability

Data will be made available on request.

Acknowledgments

This work was conducted with generous financial support from Woodard & Curran and the Strategic Environmental Research and Development Program (SERDP) under Project ER21-1129 (contract number W912HQ-22-C-0033): “Experimental Evaluation and Mathematical Modeling of Particulate Amendment Delivery, Retention and Adsorption Performance in the Subsurface”. The content of this manuscript has not undergone SERDP review, and no official endorsement should be inferred.

Appendix A. Supplementary data

Supplementary data to this article can be found online at <https://doi.org/10.1016/j.chemosphere.2024.143331>.

References

- Abunada, Z., Alazaiza, M.Y., Bashir, M.J., 2020. An overview of per-and polyfluoroalkyl substances (PFAS) in the environment: source, fate, risk and regulations. *Water* 12, 3590. <https://doi.org/10.3390/w12123590>.
- Alhashimi, H.A., Aktas, C.B., 2017. Life cycle environmental and economic performance of biochar compared with activated carbon: a meta-analysis. *RCR Advances* 118, 13–26. <https://doi.org/10.1016/j.resconrec.2016.11.016>.
- Appleman, T.D., Dickenson, E.R., Bellona, C., Higgins, C.P., 2013. Nanofiltration and granular activated carbon treatment of perfluoroalkyl acids. *J. Hazard Mater.* 260, 740–746. <https://doi.org/10.1016/j.jhazmat.2013.06.033>.
- Appleman, T.D., Higgins, C.P., Quiñones, O., Vanderford, B.J., Kolstad, C., Zeigler-Holady, J.C., Dickenson, E.R., 2014. Treatment of poly-and perfluoroalkyl substances in US full-scale water treatment systems. *Water Res.* 51, 246–255. <https://doi.org/10.1016/j.watres.2013.10.067>.
- Askeland, M., Clarke, B.O., Cheema, S.A., Mendez, A., Gasco, G., Paz-Ferreiro, J., 2020. Biochar sorption of PFOS, PFOA, PFHxS and PFHxA in two soils with contrasting texture. *Chemosphere* 249, 126072. <https://doi.org/10.1016/j.chemosphere.2020.126072>.
- Becanova, J., Saleeba, Z.S., Stone, A., Rubock, A.R., Hurt, R.H., Lohmann, R., 2021. A graphene-based hydrogel monolith with tailored surface chemistry for PFAS passive sampling. *Environ. Sci.: Nano* 8, 2894–2907. <https://doi.org/10.1039/D1EN00517K>.
- Begley, T., White, K., Honigfort, P., Twaroski, M., Neches, R., Walker, R., 2005. Perfluorochemicals: potential sources of and migration from food packaging. *Food Addit. Contam.* 22, 1023–1031. <https://doi.org/10.1080/02652030500183474>.
- Boyer, T.H., Fang, Y., Ellis, A., Dietz, R., Choi, Y.J., Schaefer, C.E., Higgins, C.P., Strathmann, T.J., 2021. Anion exchange resin removal of per-and polyfluoroalkyl substances (PFAS) from impacted water: a critical review. *Water Res.* 200, 117244. <https://doi.org/10.1016/j.watres.2021.117244>.
- Cantoni, B., Turolla, A., Wellnitz, J., Ruhl, A.S., Antonelli, M., 2021. Perfluoroalkyl substances (PFAS) adsorption in drinking water by granular activated carbon: influence of activated carbon and PFAS characteristics. *Sci. Total Environ.* 795, 148821. <https://doi.org/10.1016/j.scitotenv.2021.148821>.
- Chen, X., Xia, X., Wang, X., Qiao, J., Chen, H., 2011. A comparative study on sorption of perfluorooctane sulfonate (PFOS) by chars, ash and carbon nanotubes. *Chemosphere* 83, 1313–1319. <https://doi.org/10.1016/j.chemosphere.2011.04.018>.
- Deng, S., Nie, Y., Du, Z., Huang, Q., Meng, P., Wang, B., Huang, J., Yu, G., 2015. Enhanced adsorption of perfluorooctane sulfonate and perfluorooctanoate by bamboo-derived granular activated carbon. *J. Hazard Mater.* 282, 150–157. <https://doi.org/10.1016/j.jhazmat.2014.03.045>.
- Dixit, F., Dutta, R., Barbeau, B., Berube, P., Mohseni, M., 2021. PFAS removal by ion exchange resins: a review. *Chemosphere* 272, 129777. <https://doi.org/10.1016/j.chemosphere.2021.129777>.
- Du, Z., Deng, S., Bei, Y., Huang, Q., Wang, B., Huang, J., Yu, G., 2014. Adsorption behavior and mechanism of perfluorinated compounds on various adsorbents—a review. *J. Hazard Mater.* 274, 443–454. <https://doi.org/10.1016/j.jhazmat.2014.04.038>.
- Edeh, I.G., Mašek, O., 2022. The role of biochar particle size and hydrophobicity in improving soil hydraulic properties. *Eur. J. Soil Sci.* 73, e13138.
- Fotouhi, F., Kresic, N., 2010. *Springwater Treatment. Groundwater Hydrology of Springs*. Elsevier, pp. 269–304.
- Franke, V., McCleef, P., Lindgren, K., Ahrens, L., 2019. Efficient removal of per-and polyfluoroalkyl substances (PFAS) in drinking water treatment: nanofiltration combined with active carbon or anion exchange. *Environ. Sci.: Water Res. Technol.* 5, 1836–1843. <https://doi.org/10.1039/C9EW00286C>.
- Gagliano, E., Sgroi, M., Falciglia, P.P., Vagliasindi, F.G., Roccaro, P., 2020. Removal of poly-and perfluoroalkyl substances (PFAS) from water by adsorption: role of PFAS chain length, effect of organic matter and challenges in adsorbent regeneration. *Water Res.* 171, 115381. <https://doi.org/10.1016/j.watres.2019.115381>.
- Gao, Y., Deng, S., Du, Z., Liu, K., Yu, G., 2017. Adsorptive removal of emerging polyfluoroalkyl substances F-53B and PFOS by anion-exchange resin: a comparative study. *J. Hazard Mater.* 323, 550–557. <https://doi.org/10.1016/j.jhazmat.2016.04.069>.
- Glüge, J., Scherlinger, M., Cousins, I.T., DeWitt, J.C., Goldenman, G., Herzke, D., Lohmann, R., Ng, C.A., Trier, X., Wang, Z., 2020. An overview of the uses of per- and polyfluoroalkyl substances (PFAS). *Environmental Science: Process. Impacts* 22, 2345–2373. <https://doi.org/10.1039/D0EM00291G>.
- Guo, W., Huo, S., Feng, J., Lu, X., 2017. Adsorption of perfluorooctane sulfonate (PFOS) on corn straw-derived biochar prepared at different pyrolytic temperatures. *J. Taiwan Inst. Chem. Eng.* 78, 265–271. <https://doi.org/10.1016/j.jtice.2017.06.013>.
- Hansen, M.C., Børresen, M.H., Schlabach, M., Cornelissen, G., 2010. Sorption of perfluorinated compounds from contaminated water to activated carbon. *JSS* 10, 179–185. <https://doi.org/10.1007/s11368-009-0172-z>.
- Hassan, M., Liu, Y., Naidu, R., Du, J., Qi, F., 2020. Adsorption of Perfluorooctane sulfonate (PFOS) onto metal oxides modified biochar. *Environ. Technol. Innov.* 19, 100816. <https://doi.org/10.1016/j.eti.2020.100816>.
- Hughes, S.G., 2023. PFAS in biosolids: a review of state efforts & opportunities for action. *The Environmental Council of the States, ecos. Org.* p. 29.
- Im, S.-J., Lee, H., Jang, A., 2021. Effects of co-existence of organic matter and microplastics on the rejection of PFCs by forward osmosis membrane. *Environ. Res.* 194, 110597. <https://doi.org/10.1016/j.envres.2020.110597>.
- Jha, G., Kankarla, V., McLennon, E., Pal, S., Sihi, D., Dari, B., Diaz, D., Nocco, M., 2021. Per-and polyfluoroalkyl substances (PFAS) in integrated crop-livestock systems: environmental exposure and human health risks. *Int. J. Environ. Res. Public Health* 18, 12550. <https://doi.org/10.3390/ijerph182312550>.
- Jjagwe, J., Olupot, P.W., Meny, E., Kalibbala, H.M., 2021. Synthesis and application of Granular activated carbon from biomass waste materials for water treatment: a review. *J. Bioresour. Bioprod.* 6, 292–322. <https://doi.org/10.1016/j.jobab.2021.03.003>.
- Keller, A.A., Li, W., Floyd, Y., Bae, J., Clemens, K.M., Thomas, E., Han, Z., Adeleye, A.S., 2024. Elimination of microplastics, PFAS, and PPCPs from biosolids via pyrolysis to produce biochar: feasibility and techno-economic analysis. *Sci. Total Environ.*, 174773. <https://doi.org/10.1016/j.scitotenv.2024.174773>.
- Kinney, T., Masiello, C., Dugan, B., Hockaday, W., Dean, M., Zygourakis, K., Barnes, R., 2012. Hydrologic properties of biochars produced at different temperatures. *Biomass Bioenergy* 41, 34–43.
- Kissa, E., 2001. *Fluorinated Surfactants and Repellents*. CRC Press.
- Krahn, K.M., Cornelissen, G., Castro, G., Arp, H.P.H., Asimakopoulos, A.G., Wolf, R., Holmstad, R., Zimmerman, A.R., Sørmo, E., 2023. Sewage sludge biochars as effective PFAS-sorbents. *J. Hazard Mater.* 445, 130449. <https://doi.org/10.1016/j.jhazmat.2022.130449>.
- Krebsbach, S., He, J., Adhikari, S., Olshansky, Y., Feyzbar, F., Davis, L.C., Oh, T.-S., Wang, D., 2023a. Mechanistic understanding of perfluorooctane sulfonate (PFOS) sorption by biochars. *Chemosphere* 330, 138661. <https://doi.org/10.1016/j.chemosphere.2023.138661>.
- Krebsbach, S., He, J., Oh, T.-S., Wang, D., 2023b. Effects of environmental factors on the sorption of per-and polyfluoroalkyl substances by biochars. *ACS ES&T Water* 3, 3437–3446. <https://doi.org/10.1021/acsestwater.3c00458>.
- Kundu, S., Patel, S., Halder, P., Patel, T., Marzbali, M.H., Pramanik, B.K., Paz-Ferreiro, J., de Figueiredo, C.C., Bergmann, D., Surapaneni, A., 2021. Removal of PFASs from biosolids using a semi-pilot scale pyrolysis reactor and the application of biosolids derived biochar for the removal of PFASs from contaminated water. *Environ. Sci.: Water Res. Technol.* 7, 638–649. <https://doi.org/10.1039/D0EW00763C>.
- Lastoskie, C., Gubbins, K.E., Quirk, N., 1993. Pore size heterogeneity and the carbon slit pore: a density functional theory model. *Langmuir* 9, 2693–2702.
- Letej, J., Carrillo, M., Pang, X., 2000. Approaches to characterize the degree of water repellency. *J. Hydrol.* 231, 61–65.

- Liu, C., Chu, J., Cápiro, N.L., Fortner, J.D., Pennell, K.D., 2022. In-situ sequestration of perfluoroalkyl substances using polymer-stabilized ion exchange resin. *J. Hazard Mater.* 422, 126960 <https://doi.org/10.1016/j.jhazmat.2021.126960>.
- Lowell, S., Shields, J.E., Thomas, M.A., Thommes, M., 2006. *Characterization of Porous Solids and Powders: Surface Area, Pore Size and Density*. Springer Science & Business Media.
- Maimaiti, A., Deng, S., Meng, P., Wang, W., Wang, B., Huang, J., Wang, Y., Yu, G., 2018. Competitive adsorption of perfluoroalkyl substances on anion exchange resins in simulated AFFF-impacted groundwater. *Chem. Eng. J.* 348, 494–502. <https://doi.org/10.1016/j.cej.2018.05.006>.
- McCleaf, P., Englund, S., Östlund, A., Lindegren, K., Wiberg, K., Ahrens, L., 2017. Removal efficiency of multiple poly-and perfluoroalkyl substances (PFASs) in drinking water using granular activated carbon (GAC) and anion exchange (AE) column tests. *Water Res.* 120, 77–87. <https://doi.org/10.1016/j.watres.2017.04.057>.
- Medina, R., Pannu, M.W., Grieco, S.A., Hwang, M., Pham, C., Plumlee, M.H., 2022. Pilot-scale comparison of granular activated carbons, ion exchange, and alternative adsorbents for per-and polyfluoroalkyl substances removal. *AWWA Water Sci* 4, e1308. <https://doi.org/10.1002/aws2.1308>.
- Murray, C.C., Marshall, R.E., Liu, C.J., Vatankhah, H., Bellona, C.L., 2021. PFAS treatment with granular activated carbon and ion exchange resin: comparing chain length, empty bed contact time, and cost. *J. Water Process Eng.* 44, 102342 <https://doi.org/10.1016/j.jwpe.2021.102342>.
- Ochoa-Herrera, V., Sierra-Alvarez, R., 2008. Removal of perfluorinated surfactants by sorption onto granular activated carbon, zeolite and sludge. *Chemosphere* 72, 1588–1593. <https://doi.org/10.1016/j.chemosphere.2008.04.029>.
- Riegel, M., Haist-Gulde, B., Sacher, F., 2023. Sorptive removal of short-chain perfluoroalkyl substances (PFAS) during drinking water treatment using activated carbon and anion exchanger. *Environ. Sci. Eur.* 35, 1–12. <https://doi.org/10.1186/s12302-023-00716-5>.
- Rodrigo, P.M., Navarathna, C., Pham, M.T., McClain, S.J., Stokes, S., Zhang, X., Perez, F., Gunatilake, S.R., Karunanayake, A.G., Anderson, R., 2022. Batch and fixed bed sorption of low to moderate concentrations of aqueous per-and poly-fluoroalkyl substances (PFAS) on Douglas fir biochar and its Fe₃O₄ hybrids. *Chemosphere* 308, 136155. <https://doi.org/10.1016/j.chemosphere.2022.136155>.
- Schuricht, F., Borovinskaya, E.S., Reschetilowski, W., 2017. Removal of perfluorinated surfactants from wastewater by adsorption and ion exchange—influence of material properties, sorption mechanism and modeling. *J. Environ. Sci.* 54, 160–170. <https://doi.org/10.1016/j.jes.2016.06.011>.
- Sinclair, G.M., Long, S.M., Jones, O.A., 2020. What are the effects of PFAS exposure at environmentally relevant concentrations? *Chemosphere* 258, 127340. <https://doi.org/10.1016/j.chemosphere.2020.127340>.
- Sonmez Baghirzade, B., Zhang, Y., Reuther, J.F., Saleh, N.B., Venkatesan, A.K., Apul, O. G., 2021. Thermal regeneration of spent granular activated carbon presents an opportunity to break the forever PFAS cycle. *Environ. Sci. Technol.* 55, 5608–5619. <https://doi.org/10.1021/acs.est.0c08224>.
- Soonmin, H., Kabbashi, N.A., 2021. Review on activated carbon: synthesis, properties and applications. *Int. J. Eng. Trends Technol.* 69, 124–139. <https://doi.org/10.14445/22315381/IJETT-V69I9P216>.
- Sørmo, E., Castro, G., Hubert, M., Licul-Kucera, V., Quintanilla, M., Asimakopoulos, A.G., Cornelissen, G., Arp, H.P.H., 2023. The decomposition and emission factors of a wide range of PFAS in diverse, contaminated organic waste fractions undergoing dry pyrolysis. *J. Hazard Mater.* 454, 131447 <https://doi.org/10.1016/j.jhazmat.2023.131447>.
- Sørmo, E., Silvani, L., Bjerklø, N., Hagemann, N., Zimmerman, A.R., Hale, S.E., Hansen, C. B., Hartnik, T., Cornelissen, G., 2021. Stabilization of PFAS-contaminated soil with activated biochar. *Sci. Total Environ.* 763, 144034 <https://doi.org/10.1016/j.scitotenv.2020.144034>.
- Thompson, K.A., Shimabuku, K.K., Kearns, J.P., Knappe, D.R., Summers, R.S., Cook, S. M., 2016. Environmental comparison of biochar and activated carbon for tertiary wastewater treatment. *Environ. Sci. Technol.* 50, 11253–11262. <https://doi.org/10.1021/acs.est.6b03239>.
- United States Environmental Protection Agency, 2018. *Reducing PFAS in Drinking Water with Treatment Technologies*. United States Environmental Protection Agency epa.gov.
- United States Environmental Protection Agency, 2022. *PFAS Treatment in Drinking Water and Wastewater- State of the Science*. United States Environmental Protection Agency. EPA Research to Support States.
- United States Environmental Protection Agency, 2023. *Proposed PFAS National Primary Drinking Water Regulation. Per- and Polyfluoroalkyl Substances (PFAS)*. United States Environmental Protection Agency epa.gov.
- Wisconsin Department of Health Services, 2023. *Chemicals: Perfluoroalkyl and Polyfluoroalkyl (PFAS) Substances*. Wisconsin Department of Health Services dhs.wisconsin.gov.
- Woodard, S., Berry, J., Newman, B., 2017. Ion exchange resin for PFAS removal and pilot test comparison to GAC. *Rem. J* 27, 19–27. <https://doi.org/10.1002/rem.21515>.
- Xiao, X., Ulrich, B.A., Chen, B., Higgins, C.P., 2017. Sorption of poly-and perfluoroalkyl substances (PFASs) relevant to aqueous film-forming foam (AFFF)-impacted groundwater by biochars and activated carbon. *Environ. Sci. Technol.* 51, 6342–6351. <https://doi.org/10.1021/acs.est.7b00970>.
- Yadav, S., Ibrar, I., Al-Juboori, R.A., Singh, L., Ganbat, N., Kazwini, T., Karbassiyazdi, E., Samal, A.K., Subbiah, S., Altaee, A., 2022. Updated review on emerging technologies for PFAS contaminated water treatment. *Chem. Eng. Res. Des.* 182, 667–700. <https://doi.org/10.1016/j.cherd.2022.04.009>.
- Yu, Q., Zhang, R., Deng, S., Huang, J., Yu, G., 2009. Sorption of perfluorooctane sulfonate and perfluorooctanoate on activated carbons and resin: kinetic and isotherm study. *Water Res.* 43, 1150–1158. <https://doi.org/10.1016/j.watres.2008.12.001>.
- Zaggia, A., Conte, L., Falletti, L., Fant, M., Chiorboli, A., 2016. Use of strong anion exchange resins for the removal of perfluoroalkylated substances from contaminated drinking water in batch and continuous pilot plants. *Water Res.* 91, 137–146. <https://doi.org/10.1016/j.watres.2015.12.039>.
- Zhang, D., Luo, Q., Gao, B., Chiang, S.-Y.D., Woodward, D., Huang, Q., 2016. Sorption of perfluorooctanoic acid, perfluorooctane sulfonate and perfluoroheptanoic acid on granular activated carbon. *Chemosphere* 144, 2336–2342. <https://doi.org/10.1016/j.chemosphere.2015.10.124>.